minerals

MDPI

Article

LA-ICP-MS Analysis of Minerals from the Shizhuyuan W-Polymetallic Deposit, South China: Implications for Mineralization of Pb, W, Mo and Bi

Jiaxin Yuan [1], Qingye Hou [1,*], Zhongfang Yang [1], Zhaochu Hu [2] and Tao Yu [1]

[1] School of Earth Sciences and Resources, China University of Geosciences, Beijing 100083, China; jiaxiny93@163.com (J.Y.); yangzf@cugb.edu.cn (Z.Y.); yutao@cugb.edu.cn (T.Y.)

[2] State Key Laboratory of Geological Processes and Mineral Resources, China University of Geosciences, Wuhan 430074, China; zchu@vip.sina.com

* Correspondence: qingyehou@cugb.edu.cn; Tel.: +86-10-82322079

Received: 31 July 2020; Accepted: 19 August 2020; Published: 24 August 2020

Abstract: The South China Block (SCB) is a globally important metallogenic district containing numerous W-Sn deposits. Extensive studies of W-polymetallic deposits in this region have greatly improved our understanding of the petrogenesis, geochronology and metallogenesis of these systems. However, studies on the mobilization of ore-forming elements between mineralization- and alteration-related minerals using in situ analyses are rare. Using laser ablation-inductively coupled plasma-mass spectrometry (LA-ICP-MS), we analyzed W, Pb, Mo and Bi concentrations in silicate minerals and scheelite from granites and skarns associated with the Shizhuyuan W-polymetallic deposit in the Nanling Range in the SCB. Data show that muscovitized biotite in granites contains high W contents. Pb mainly occurs in K-feldspar and plagioclase in granites and epidote and scheelite in skarns. Bi mainly occurs in epidote in skarns. Scheelite in skarns contains high W and Mo contents. Pb isomorphously substitutes K or Ca in silicate minerals and scheelite. W isomorphously substitutes Ti in biotite. Mo isomorphously substitutes W in scheelite and occurs as W-bearing submicroscopic inclusions in minerals with low contents. Bi isomorphously substitutes Pb when the Pb content is relatively high and occurs as Bi-bearing micro or submicroscopic inclusions in minerals when the Pb content is low. Biotite and feldspar are altered in a magmatic-hydrothermal process, W enriched in biotite, Pb enriched in feldspar and the W-, Pb-, Mo- and Bi-bearing submicroscopic inclusions are excluded from minerals and released to the magmatic-hydrothermal fluids. Large amounts of W are precipitated in scheelite when the fluids come in contact with carbonate rocks to form skarn, while a few contents of Pb, Mo and Bi are distributed in skarn minerals. Thus, large amounts of Pb, Mo, Bi and residual W remain in the fluids, which results in the formation of a W-Sn-Mo-Bi massive skarn ore.

Keywords: Pb; W; Mo; Bi; minerals; Shizhuyuan W-polymetallic deposit

1. Introduction

The South China Block (SCB), with most of the deposits formed during the Mesozoic era, has been recognized as one of the most important W-Sn metallogenic districts in the world [1]. It was formed by the amalgamation of the Yangtze Block and Cathaysia Block during the Neoproterozoic era (Figure 1a) and hosts numerous W-Sn deposits, which are mostly concentrated in the Nanling Range located in the central part of the SCB [2–4]. The Nanling Range is well known worldwide for its large-scale Mesozoic magmatism and genetically related W-Sn polymetallic deposits, which account for more than 50% of all Chinese W-Sn resources [5–7]. Some of the large, world-class deposits in the Nanling Range include the Shizhuyuan W-polymetallic deposit, Xintianling W-Mo deposit, Furong Sn

deposit, Hongqiling Sn-W-Pb-Zn deposit and Xianghualing Sn-Pb-Zn deposit [8–13], among which the Shizhuyuan W-polymetallic deposit is one of the largest polymetallic deposits in the world with giant W-Sn-Mo-Bi sources [7,14,15]. Extensive studies of these polymetallic deposits over the past few decades have greatly improved our understanding of their petrogenesis, geochronology, geochemistry and metallogenesis [3,4,16–21]. Although we have previously discussed the distribution and mobilization of Sn in the Shizhuyuan W-polymetallic deposit [13], studies on other trace element occurrences in minerals and mobilization between minerals and their alteration products are still insufficient and could improve and deepen the understanding of W mineralization of giant ore accumulations.

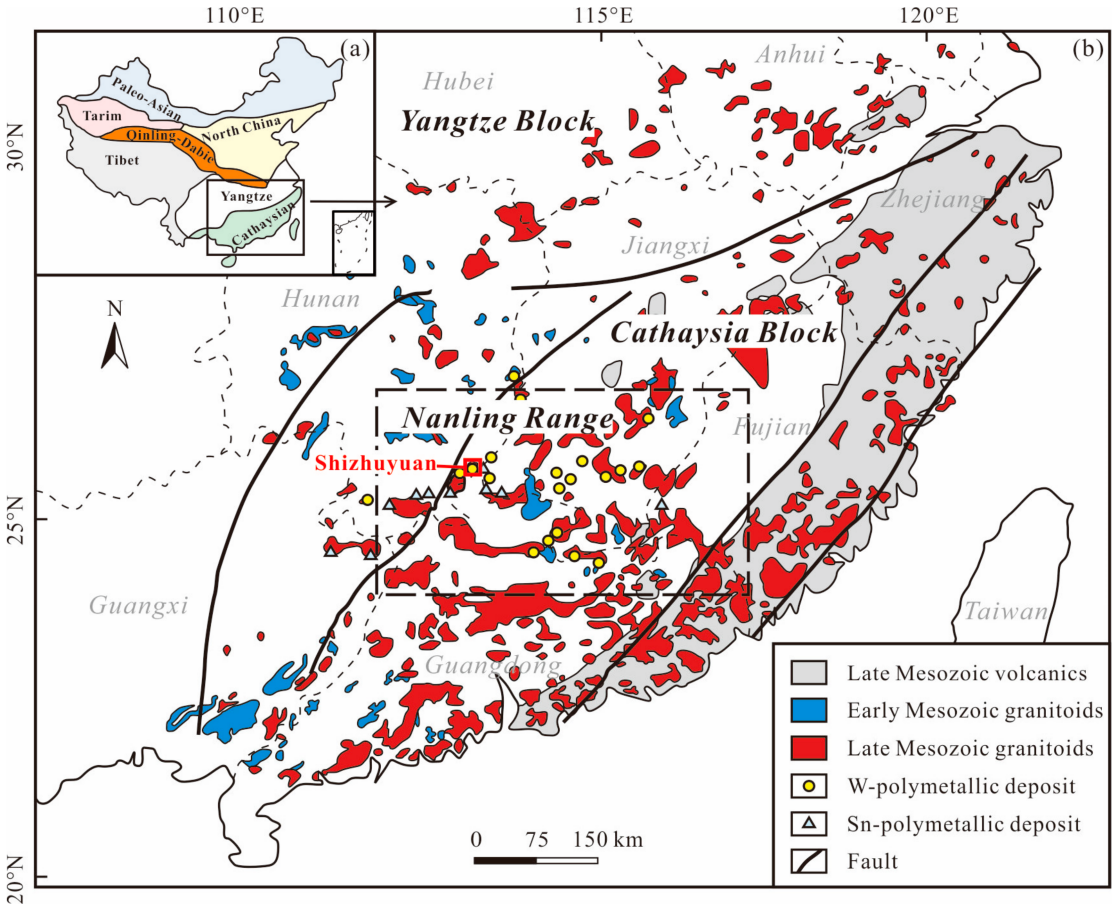

Figure 1. (**a**) Simplified tectonic outline of China where the South China Block (SCB) is separated into the Yangtze Block and the Cathaysia Block; (**b**) Geological sketch map of the SCB showing the distribution of Mesozoic granites and the Nanling Range with numerous W-Sn polymetallic deposits (modified after Chen et al. [16] and Jiang et al. [22]).

The development of laser ablation-inductively coupled plasma-mass spectrometry (LA-ICP-MS) allows in situ micro analysis of a large number of trace elements with relatively low detection limits (~1 ppb for a large number of trace elements [23,24]). It has been widely used to determine elemental and isotopic compositions of fluid inclusions and minerals in order to constrain magmatic and hydrothermal processes [20,25–27]. Using in situ LA-ICP-MS, Song et al. [28] studied the behavior of trace elements in scheelite and constrained ore genesis in porphyry-skarn W-Mo systems. Choi et al. [29] examined the REE patterns of scheelite, which showed the relationship between the evolution of ore-forming fluids and the formation of multistage scheelites from the W-skarn deposit. Chen et al. [30] studied the occurrences and contents in magnetite and pyrite from the Hetaoping Fe-Zn-Pb skarn deposit and suggested that the ore-forming fluid in Hetaoping was of magmatic origin.

In this paper, we present in situ LA-ICP-MS element concentration data of major silicate minerals and scheelite in granites and skarns from the Shizhuyuan W-polymetallic deposit. The variation of Pb, W, Mo and Bi contents in different granite- and skarn-hosted minerals are presented and their relative distribution are discussed to highlight the mobilization of these elements during skarn formation and mineralization. We use these data to constrain the behavior of Pb, W, Mo and Bi during mineralization processes in order to improve our understanding of the distribution, migration and mineralization of these trace elements to form the giant deposit.

2. Geological Setting

The Nanling Range (approximately 110–116° E, 24–27° N) is located in the central SCB and covers a surface area of ca. 170,000 km^2 [7,31]. It consists of strongly folded and metamorphosed Neoproterozoic-Ordovician flysch and volcanic basement overlain by Late Devonian to Early Triassic sedimentary rocks [2]. Mesozoic granitoid intrusions are well-developed throughout this region (Figure 1). The granitoid plutons formed by multiple cycles of tectono-magmatism are most directly associated with W-Sn-rare metal mineralization [2,32]. The Nanling Range is an important W-Sn polymetallic metallogenic province with skarn-type W-Sn polymetallic deposits dominant in the west and quartz vein-type W deposits predominant in the east [3,6,7,31].

The Shizhuyuan W-polymetallic deposit, situated in the western Nanling Range, is a world-class ore deposit containing ca. 800,000 Mt of WO_3, 486,000 Mt of Sn, 200,000 Mt of Mo and 100,000 Mt of Bi [16]. The deposit is located at the southwestern contact between the Qianlishan granite complex and Devonian carbonate rocks and marlstone (Figure 2 [9,33]). The deposit covers an area of 1200 × 600 m^2 and has a thickness of ca. 200–300 m [15]. Four major types of ores are classified based on their locations and metal species (Figure 3 [7,8,15,19]): W-Sn-Mo-Bi massive greisen ore (type I), W-Sn-Mo-Bi-F stockwork ore (type II) hosting in both greisen and skarn, W-Bi-Mo-Sn massive skarn ore (type III) and Sn-Be veinlet ore in marble (type IV).

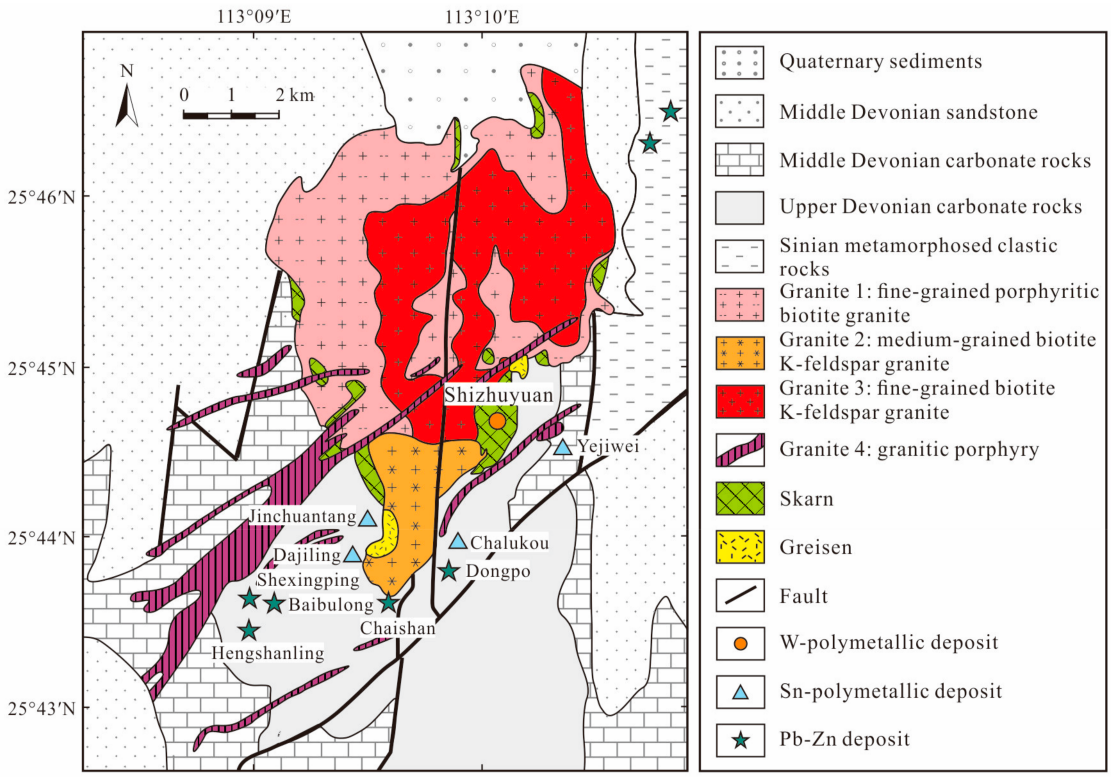

Figure 2. Schematic geological map of the Shizhuyuan W-polymetallic deposit (modified after Chen et al. [16] and Jiang et al. [19]).

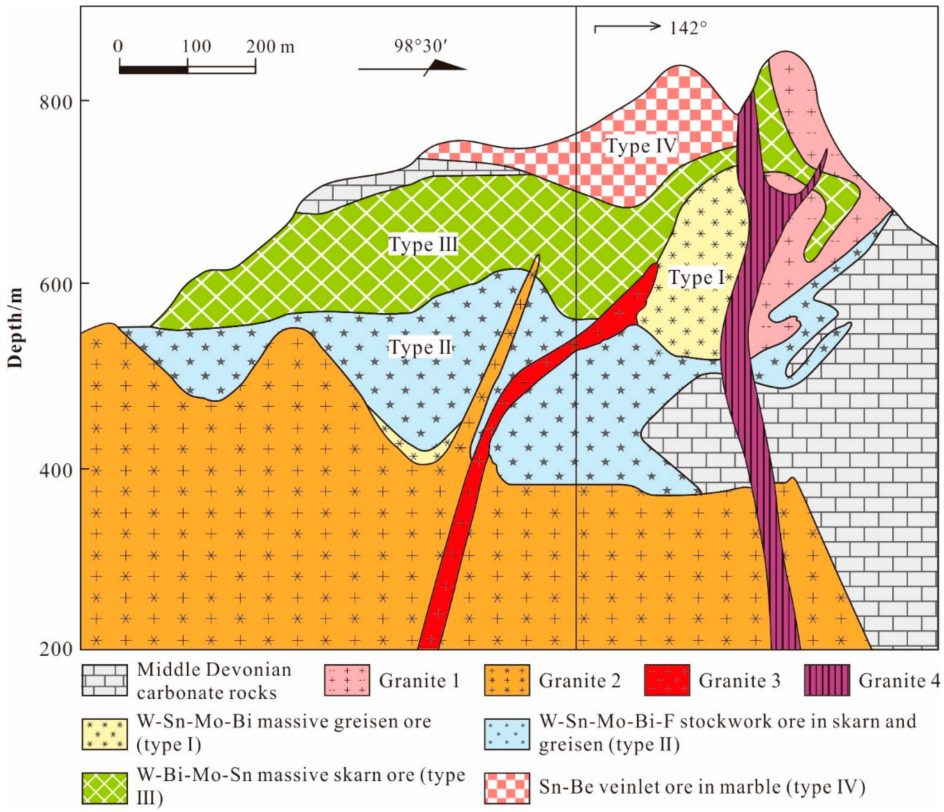

Figure 3. Drill core profile of the Shizhuyuan W-polymetallic deposit showing the position of the four main ore types (modified after Zhao et al. [7] and Lu et al. [8]).

The Shizhuyuan W-polymetallic deposit is considered to be genetically related to the Qianlishan granitic complex, with intense skarn and greisen alteration associated with the mineralization [7,34]. The Qianlishan complex mainly consists of four intrusive granitic phases: fine-grained porphyritic biotite granite (187–182 Ma) (granite 1), medium-grained biotite K-feldspar granite (162–158 Ma) (granite 2), fine-grained biotite K-feldspar granite (158–146 Ma) (granite 3) and granitic porphyry (146–144 Ma) (granite 4) (Figure 2 [8,35,36]). The Shizhuyuan skarn, dominated by a garnet skarn, lies in the contact zone between the Qianlishan granite complex and the Middle-Upper Devonian carbonate rocks [19,35]. The Devonian carbonate rocks are important ore-bearing rocks, which can be subdivided into four formations (from bottom to top): (1) the Tiaomajian Formation (>358 m thick, Middle Devonian) is composed of sandstones and conglomerates, (2) the Qiziqiao Formation (>520 m thick, Middle Devonian) mainly comprises micritic dolomites, dolomitic limestones and limestones, (3) the Shetianqiao Formation (>296 m thick, Upper Devonian) primarily consists of micritic dolomites intercalated with argillaceous bands and (4) the Xikuangshan Formation (>363 m thick, Upper Devonian) consists of limestones and dolomitic limestones [15,37]. Granite 2 was vital to the main W-Sn-Mo-Bi mineralization among the four granitic phases [7,8,19]. Granite 2 transformed the limestone into marble and a massive skarn (dominated by the garnet skarn), which has been converted into retrograde or hydrous skarn by later hydrothermal alteration [8,17]. Retrograde alteration of primary skarns occurred and was accompanied by the formation of the W-Bi-Mo-Sn massive skarn ore from magmatic-hydrothermal fluid at various stages [8].

3. Petrography

Granite 1 (fine-grained porphyritic biotite granite) is massive with phenocrysts of quartz, feldspar and biotite (Figure 4a). Granite 2 (medium-grained biotite K-feldspar granite) is mainly composed of K-feldspar, plagioclase, biotite, quartz and a few melanocratic opaque minerals (Figure 4b). Granite 3

(fine-grained biotite K-feldspar granite) dominantly consists of biotite, K-feldspar, plagioclase, quartz and a few melanocratic opaque minerals (Figure 4c). Granite 4 (granitic porphyry) is massive with a porphyritic texture, with phenocrysts primarily of quartz, feldspar and small amounts of biotite (Figure 4d). Granite samples were altered to different degrees, with some K-feldspar being altered into clay minerals, some plagioclase altered to sericite and an aggregate of clay minerals and biotite generally altered to chlorite and muscovite (Figure 4).

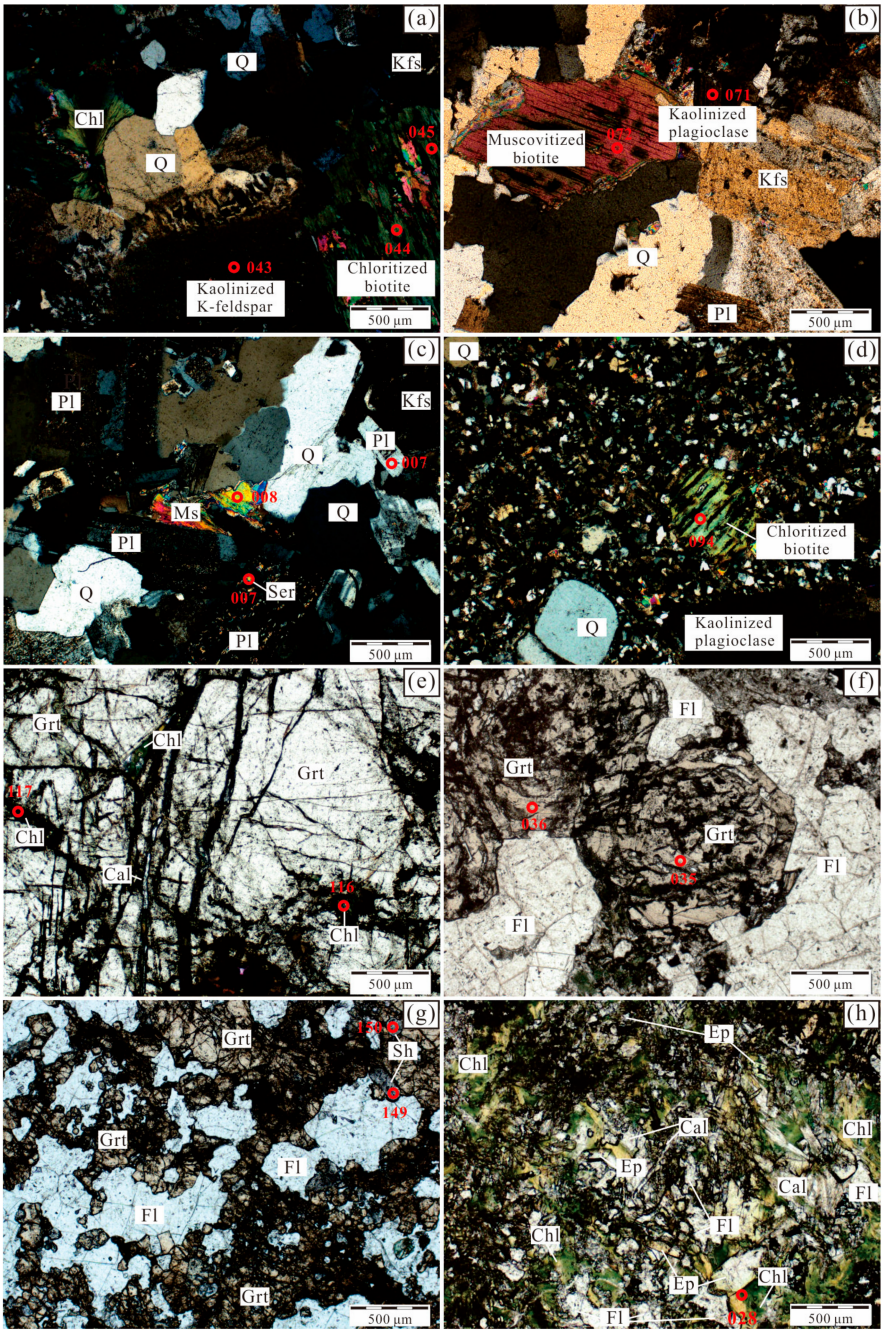

Figure 4. Photomicrographs of fresh and altered minerals in granites and skarns from the Shizhuyuan W-polymetallic deposit. (**a**) Granite 1; (**b**) Granite 2; (**c**) Granite 3; (**d**) Granite 4; (**e**) Garnet skarn; (**f**), (**g**) Fluorite-garnet skarn; (**h**) Epidote-fluorite-chlorite skarn. Q: quartz; Bi: biotite; Kfs: K-feldspar; Pl: plagioclase; Ms: muscovite; Ser: sericite; Grt: garnet; Chl: chlorite; Cal: calcite; Fl: fluorite; Ep: epidote; Sh: scheelite. The circles are LA-ICP-MS analytical spots with their numbers corresponding to those listed in Table S1.

Skarns are dominated by a garnet skarn, fluorite-garnet skarn and epidote-fluorite-garnet skarn in the Shizhuyuan deposit. The texture of the skarns varies from lepidoblastic to granoblastic with massive or mesh-vein structures. The garnet skarn consists of garnet, chlorite, epidote, calcite, fluorite and a few opaque minerals (Figure 4e). The primary minerals of the fluorite-garnet skarn include garnet, fluorite, chlorite, epidote, calcite, opaque minerals and scarce scheelite (Figure 4f,g), while those of the epidote-fluorite-chlorite skarn are epidote, chlorite, fluorite, calcite and opaque minerals (Figure 4h). The garnet was partially altered to chlorite in some thin sections of the three skarns (Figure 4e).

4. Sampling and Analytical Methods

Thirteen representative granite (granites 1–4) and skarn (garnet skarn, fluorite-garnet skarn and epidote-fluorite-chlorite skarn) samples were collected at the 490 m levels of Shizhuyuan in the Shizhuyuan ore district. One hundred and fifty-three spots of silicate minerals, alteration minerals and scheelite were selected from 13 sample thin sections for analysis.

Element concentrations were determined by LA-ICP-MS using a GeoLas 193-nm Laser Ablation system coupled with an Agilent 7500a ICP-MS instrument at the State Key Laboratory of Geological Processes and Mineral Resources, China University of Geosciences, Wuhan, China. Detailed operating conditions for the laser ablation system and the ICP-MS instrument, as well as data reduction, have been described by Liu et al. [23]. Each analysis was performed using a laser spot size of 44 μm with a pulse rate of 6 Hz and an energy of 60 MJ and started with a gas blank of approximately 20–30 s followed by data acquisition of 50 s from the sample. The element contents were calibrated against multiple reference materials (NIST 610, BCR-2G, BIR-1G and BHVO-2G) as external standards. In particular, ^{29}Si was used as an internal standard for K-feldspar, plagioclase, biotite, muscovite, garnet, epidote and chlorite, while ^{42}Ca was used as an internal standard for scheelite [23]. Major element concentrations of chloritized biotite, epidote and chloritized garnet were corrected with EMPA (Electron microprobe analysis) data (see electronic Appendix A in Yuan et al. [13]), which were obtained from polished thin sections using a JEOL JXA-8100M electron microprobe (EMP) at the Analytical Laboratory of Beijing Research Institute of Uranium Geology (BRIUG), Beijing, China. The operating conditions of the EMP included an accelerating voltage of 15 kV and a probe current of 20 nA focused to a spot of ~1 μm and a ZAF (atomic number effect, absorption effect and fluorescence effect) correction procedure for data reduction. The offline reduction of data obtained by LA-ICP-MS was performed with the program ICPMSDataCal (V9.0, State Key Laboratory of Geological Processes and Mineral Resources, China University of Geosciences, Wuhan, China) obtained from Liu et al. [23], including an integration selection of analyte signals and background, time-drift correction and quantitative calibration [23,38]. The LA-ICP-MS analytical results of major elements and W, Mo, Bi and Pb for minerals are summarized in Table S1 and the results of major elements and W, Mo, Bi and Pb for international reference materials are summarized in Table S2 (data of major elements are cited from Yuan et al. [13]). The measurement accuracy of element concentrations was better than 5% for most elements, based on repeated analyses of the reference materials.

5. Analytical Results

5.1. Major Elements

Table S3 shows the summary statistics of the major elements and Pb, W, Mo and Bi contents for K-feldspar, plagioclase, altered biotite, garnet, chlorite, epidote and scheelite from different rock samples.

Primary K-feldspar is mainly orthoclase ($Or_{81–98}$) with $Ab_{2–19}$ (albite) and lacking a significant An component (anorthite). Primary plagioclase in granites is enriched in Na_2O ($Ab_{95–99}$) with low K_2O ($Or_{0–3}$) and CaO ($An_{0–3}$) (Table S1 [13]). Biotite is generally altered to muscovite and chlorite to different degrees in granites. Among K-feldspar, plagioclase and altered biotite in granites, K-feldspar contains

higher K_2O contents, while altered biotite contains higher FeO and TiO_2 contents. Muscovitized biotite contains relatively lower FeO, K_2O and TiO_2 compared with chloritized biotite (Table S3).

Garnet in skarns represent a solid solution between andradite (42.2–62.7 mol %) and grossular (19.5–52.8 mol %), with appreciable proportions of spessartine (3.95–10.4 mol %) and pyrope (0.077–7.31 mol %) (Table S1 [13]). The CaO and WO_3 contents of scheelite in skarns range from 18.5–20.0 wt % and 73.3–80.7 wt %, respectively (Tables S1 and S3). Among garnet, epidote and chlorite in skarns, chlorite contains relatively lower CaO and higher FeO compared with garnet, epidote and scheelite (Table S3).

5.2. Pb, W, Mo and Bi

The analyses regarding Pb, W, Mo and Bi contents of main silicate minerals and scheelite are listed in Table S1 and shown in Figure 5. Table S3 contains the summary statistics of Pb, W, Mo and Bi contents for the analyzed minerals.

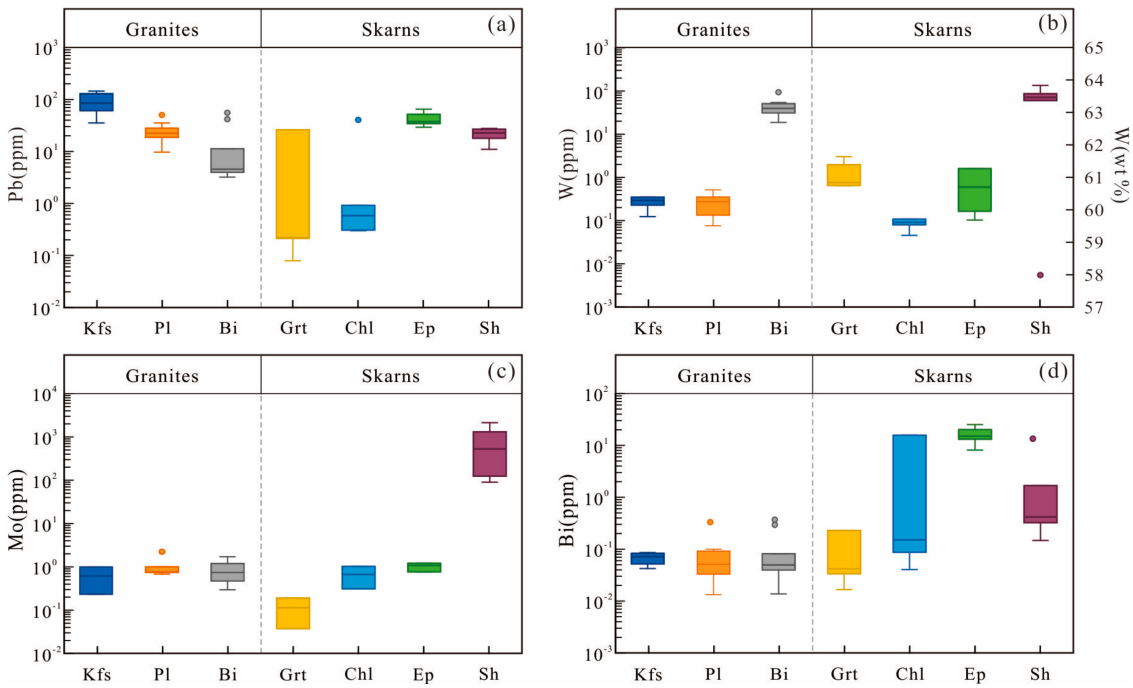

Figure 5. Box plots of (**a**) Pb, (**b**) W, (**c**) Mo and (**d**) Bi concentrations of main silicate minerals and scheelite. Kfs: K-feldspar; Pl: plagioclase; Bi: muscovitized biotite; Grt: garnet; Chl: chlorite; Ep: epidote; Sh: scheelite.

In granites, K-feldspar contains the highest Pb contents (91.9 ppm on average), whereas muscovitized biotite contains relatively high W contents (43.7 ppm on average) compared with other minerals. Mo and Bi contents are low in feldspar (<2.23 ppm and <0.22 ppm, respectively) and muscovitized biotite (<1.71 ppm and <0.24 ppm, respectively) (Figure 5, Table S3).

In skarns, epidote and scheelite have relatively high Pb (43.6 ppm and 21.2 ppm on average, respectively) and Bi contents (16.3 ppm and 1.57 ppm on average, respectively). Scheelite contains higher W and Mo contents (624,452 ppm and 838 ppm on average, respectively) compared with silicate minerals (Figure 5, Table S3).

6. Discussion

6.1. Occurrence of Pb, W, Mo and Bi

Granites are composed mainly of K-feldspar, plagioclase, altered biotite and quartz, while skarns consist mainly of garnet, chlorite, epidote and scheelite.

K-feldspar and plagioclase contain relatively high Pb contents (9.70–144 ppm) and low W (<0.53 ppm), Mo (<2.23 ppm) and Bi (<0.22 ppm) contents (Figure 5). The pure mineral would display a flat time-resolved depth profile, while the mineral inclusions usually show some peaks in time-resolved depth profiles [25,39,40]. Time-resolved depth profiles for Pb are rarely flat and covariant with Na, K and Al (major elements for feldspar), which indicates that Pb enters the crystal lattice of feldspar by isomorphic substitution (Figure 6a,b). Feldspar is a tectosilicate mineral with a general chemical formula $M[(Al,Si)_4O_8]$, where M represents ions such as Na^+, Ca^{2+}, K^+ and other trace elements (Sr^{2+}, Pb^{2+}) with a low valence state, large radius and high coordination [41]. Pb has a similar radius to K (Pb^{2+} (1.20 Å), K^+ (1.33 Å)) [42]. Thus, Pb could replace K outside the silicon-oxygen framework with the substitution reaction $Pb^{2+} + Al^{3+} \rightarrow K^+ + Si^{4+}$. Some studies have shown that Bi could enter the lattice by isomorphously substituting Pb in some minerals such as galena [43–45]. Since Pb^{2+} and Bi^{3+} have the similar radius and electronic configuration (Pb^{2+} (1.20 Å), Bi^{3+} (1.20 Å)) [42], Bi is speculated to isomorphously substitute Pb in K-feldspar and plagioclase with the substitution reaction $Bi^{3+} + Al^{3+} \rightarrow Pb^{2+} + Si^{4+}$. The concentrations of W and Mo are low (Figure 6a,b) and have no obvious correlations with other elements, implying that the analyzed W and Mo were present in the form of W- and Mo-bearing submicroscopic (invisible) inclusions in the feldspar [46].

Biotite is a TOT-type (tetrahedron-octahedron-tetrahedron) phyllosilicate mineral with the chemical formula $K\{(Mg,Fe)_3[AlSi_3O_{10}](OH)_2\}$. Al^{3+}, Fe^{3+} and Ti^{4+} often replace Mg^{2+} and Fe^{2+} at the octahedral site [47]. Ti is a common trace element in mica and has similar crystal chemical properties to W [48]. Since Ti, Sn and W are highly compatible elements in mica, mica has been considered as one of the important minerals for revealing W-Sn mineralization genetically related to granites [48,49]. In fact, Ti can enter the lattice of biotite through the isomorphous substitution equation as follows: $Ti^{4+} + 2Al^{3+} \rightarrow M^{2+} + 2Si^{4+}$ (M^{2+} could be Mg^{2+} or Fe^{2+}) [47]. Since the ionic radius of Ti^{4+} is the same as that of W^{6+} (Ti^{4+} (0.68 Å), W^{6+} (0.68 Å)) [42], W is suggested to occur in biotite as an isomorphous substitution of Ti with the substitution equation $Fe^{2+} + W^{6+} \rightarrow 2Ti^{4+}$ [50].

Garnet analyses show relatively high Pb contents (0.079–26.1 ppm) and low W, Mo and Bi contents (<3.03 ppm, <0.19 ppm and <0.23 ppm, respectively) when compared with chlorite and epidote in skarns (Figures 5 and 6c). Garnet is a nesosilicate mineral with the general chemical formula $A_3B_2[SiO_4]_3$, where A represents eight-coordinate cations (Fe^{2+}, Mg^{2+}, Ca^{2+}, Na^+ and K^+) and B represents octahedral-coordinate cations (Fe^{3+}, Ti^{4+} and Cr^{3+}) [51]. Garnet in this study is mainly a solid solution between grossular and andradite, with the chemical formula $Ca_3(Fe^{3+})_2$ $[SiO_4]_3$-$Ca_3Al_2[SiO_4]_3$ [13]. The LA-ICP-MS spectra for Pb in garnet was relatively smooth and consistent with Ca and K, indicating that Pb occurred as an isomorphous substitution in eight-coordinates with Ca and K due to the similar radius (Pb^{2+} (1.20 Å), K^+ (1.33 Å), Ca^{2+}(0.99 Å)) [42,46]. Time-resolved depth profiles for Bi, Mo and W imply the form of Bi-, Mo- and W-bearing submicroscopic inclusions in garnet (Figure 6c).

Epidote contains relatively high Pb and Bi and low W and Mo contents compared with garnet and chlorite in skarns (Figures 5 and 6d). Epidote is a nesosilicate mineral with the chemical formula $Ca_2Fe^{3+}Al_2[SiO_4][Si_2O_7]O(OH)$. It is suggested that octahedral-coordinated Pb could partially substitute for Ca due to the similar ionic radius and spectra covariation (Figure 6d). Epidote contains low Bi contents due to the substitution between Pb^{2+} and Bi^{3+} (Figure 6d). W and Mo occur as W- and Mo-bearing submicroscopic inclusions residing in epidote.

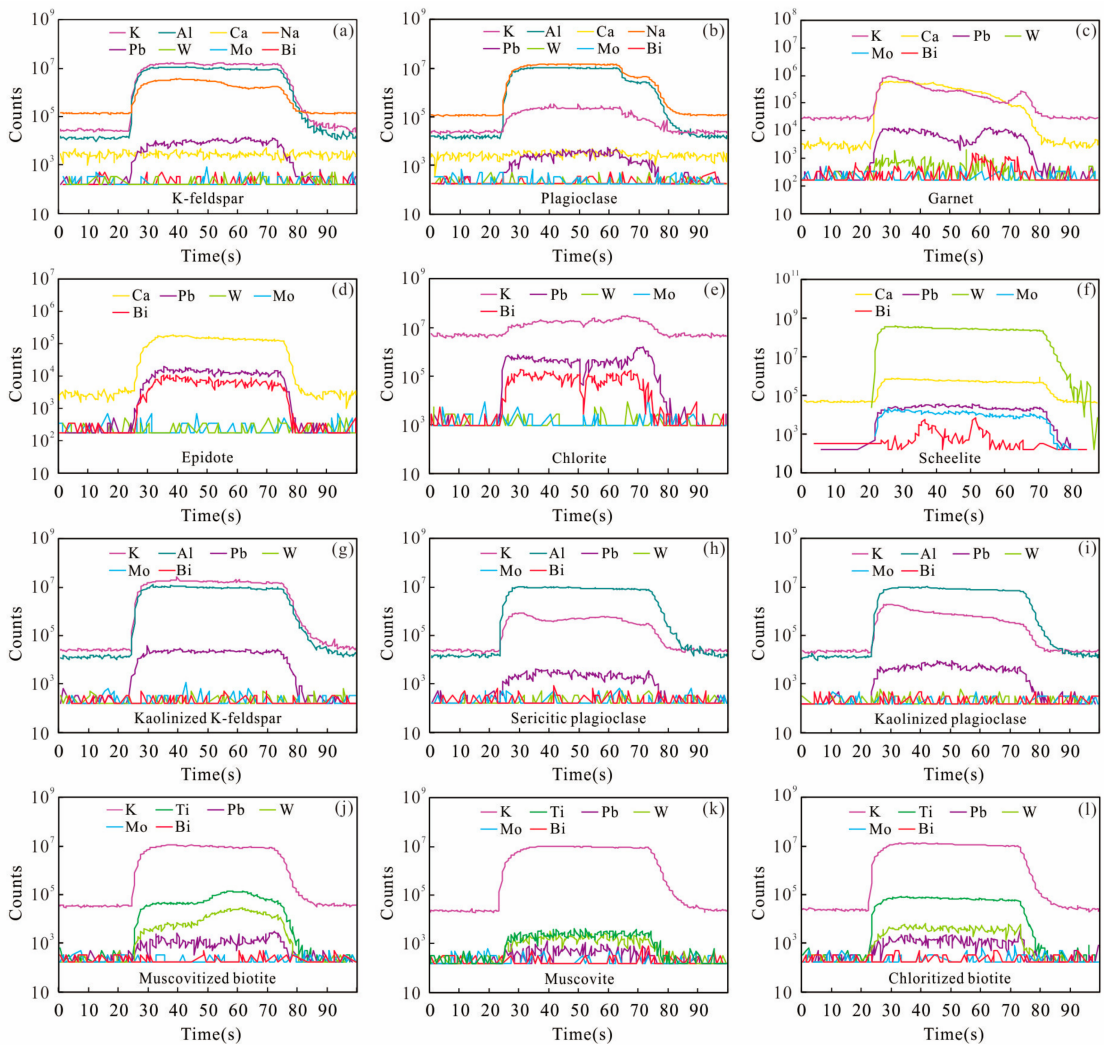

Figure 6. Representative time-resolved LA-ICP-MS depth profiles for minerals indicating the occurrences of Pb, W, Mo, Bi and other major elements. (**a**) K-feldspar (spot number 076); (**b**) Plagioclase (spot number 006); (**c**) Garnet (spot number 035); (**d**) Epidote (spot number 029); (**e**) Chlorite (spot number 025); (**f**) Scheelite (spot number 150); (**g**) Kaolinized K-feldspar (spot number 055); (**h**) Sericitic plagioclase (spot number 018); (**i**) Kaolinized plagioclase (spot number 014); (**j**) Muscovitized biotite (spot number 128); (**k**) Muscovite (spot number 010); (**l**) Chloritized biotite (spot number 086).

The concentrations of Pb, W, Mo and Bi are relatively low in chlorite in skarns (Figure 5). Chlorite is a phyllosilicate mineral and its ideal structure is characterized by TOT sheets and regularly alternating octahedral sheets [52]. The general chemical formula of chlorite is $Y_x[T_4O_{10}](OH)_8$, in which the letter Y represents the octahedral-coordinated cations, such as Al^{3+}, Mg^{2+}, Fe^{2+} and Fe^{3+} and the letter T represents the tetrahedral-coordinated cations, such as Si^{4+} and Al^{3+} [53,54]. Time-resolved depth profiles for Pb and Bi were rather smooth and consistent, demonstrating the occurrences as isomorphisms in chlorite (Figure 6e). The major elements Fe, Mg and Al in chlorite have large differences in ionic radius in relation to Pb (Fe^{2+} (0.76 Å), Mg^{2+} (0.60 Å), Al^{3+} (0.50 Å), Pb^{2+} (1.20 Å)) [42], therefore Pb generally does not isomorphously substitute with them in chlorite. The flat spectra of Pb and the covariation with K indicate that Pb occurred as an isomorphous substitution of K (Figure 6e). The Pb content was rather low due to the low K_2O concentration (0.0071–0.075 wt %). Chlorite contains few Bi contents due to the isomorphism between Pb^{2+} and Bi^{3+} (Figure 6e).

Scheelite has remarkably high Mo contents (Figure 5c). Scheelite is a calcium tungstate mineral in the tetragonal crystal system with the chemical formula $CaWO_4$. Scheelite has a simple crystal structure

with irregular dodecahedral $[CaO_8]^{14-}$ (which can accommodate alkaline earths and alkalis such as Ca^{2+} and Na^{+}) and tetrahedral $[WO_4]^{2-}$ sites (which can accommodate highly charged, smaller cations such as W^{6+} and Mo^{6+}) [55]. Furthermore, W and Mo had a common evolutionary trend during the magmatic evolution due to the similar chemical properties regarding ionic radius, ionic valence state and electronegativity [56–58]. Scheelite contains few Pb contents due to the substitution between Pb^{2+} and Ca^{2+} (Figure 6f). Some spectra of Bi in scheelite are rather flat, while some spectra show peaks, which demonstrates that Bi occurs both as Bi-bearing micro inclusions and isomorphous substitution in scheelite through the equation as follows: $Ca^{2+} + W^{6+} \rightarrow Bi^{3+} + V^{5+}$ [59] (Figure 6f).

6.2. Mobilization of Pb, W, Mo and Bi During Alteration

6.2.1. Alteration of K-feldspar

Parts of K-feldspar in granites are cloudy and dirty on the surface and locally have transitioned into clay minerals (Figure 4a). As K-feldspar is generally altered to kaolinite during the process of hydrothermal alteration [60,61], the clay minerals in this study are all treated as kaolinites. The alteration reaction is as follows [60]:

$$4K[AlSi_3O_8]\ (\text{K-feldspar}) + H_2O + 2CO_2 \rightarrow Al_4[Si_4O_{10}](OH)_8\ (\text{kaolinite}) + 8SiO_2 + 4K^+ + 2CO_3{}^{2-}$$

Major element contents of kaolinized K-feldspar and K-feldspar show little variation, with the exception of Al (Table S3; 18.7–20.4 wt % for K-feldspar and 14.6–47.0 wt % for kaolinized K-feldspar, respectively). Pb content decreased slightly during the alteration, while Bi content was almost unchanged (Figure 7a,d). Both K-feldspar and kaolinized K-feldspar are depleted in W and Mo (Figure 7b,c). Due to the similar ionic radius, Pb occurs in the lattice of K-feldspar and kaolinized K-feldspar as an isomorphous substitution for K (Figure 6g). Kaolinite is an abundant micro and submicrometer-sized sheet silicate mineral $[Al_4Si_4O_{10}(OH)_8]$ built up of alternating tetrahedral (T) and octahedral (O) sheets with no interlayer space [62]. When K-feldspar is altered to kaolinite, $[AlO_4]$ is replaced by $[SiO_4]$ and K^+ is replaced by Al^{3+} on the octahedral site and K content decreases overall [61,63], therefore Pb is also excluded from the mineral lattice due to isomorphous substitution. Thus, the more intensely K-feldspar alters to kaolinite, the more K and Pb are released into the magmatic-hydrothermal fluids. As Bi isomorphously substitutes Pb in K-feldspar, Bi is also excluded from the feldspar mineral lattice and may enter fluids when K-feldspar alters to kaolinite. W, Mo and the residual Bi may occur as W-, Mo- and Bi-bearing submicroscopic inclusions residing in kaolinized K-feldspar considering their jagged spectra (Figure 6g).

6.2.2. Alteration of Plagioclase

Parts of plagioclase in granites are altered to sericite and clay minerals (Figure 4c,d). Sericite is a fine-grained flaky aggregate of muscovite. The sericitization of plagioclase is as follows [64]:

$$6NaAlSi_3O_8\ (\text{plagioclase}) + 2H_2O + 2CO_2 + 2K^+ \rightarrow 2KAl_2[AlSi_3O_{10}][OH]_2\ (\text{sericite}) + 12SiO_2 + 6Na^+ + CO_3{}^{2-}$$

The K_2O, Al_2O_3 and FeO contents are higher in sericitic plagioclase than in fresh plagioclase (Table S3). During the sericitization of plagioclase, Pb contents decrease, while W, Mo and Bi contents remain relatively low and almost unchanged (Figure 7). Sericitic plagioclase contains low Pb and Bi contents due to the substitution between K^+, Pb^{2+} and Bi^{3+}, respectively (Figure 6h).

Parts of plagioclase are cloudy on the surface and transitioned into kaolinite through the reaction [65]:

$$2Na[AlSi_3O_8]\ (\text{plagioclase}) + H_2O + 2H^+ \rightarrow Al_2[Si_2O_5](OH)_4\ (\text{kaolinite}) + 4SiO_2 + 2Na^+$$

The differences regarding Pb, W, Mo and Bi between kaolinized plagioclase and plagioclase are negligible (Figure 7). Moreover, Pb could enter the lattice of kaolinized plagioclase as an isomorphous substitution of K, while W, Mo and Bi may occur as W-, Mo- and Bi-bearing submicroscopic inclusions residing in the minerals (Figure 6i).

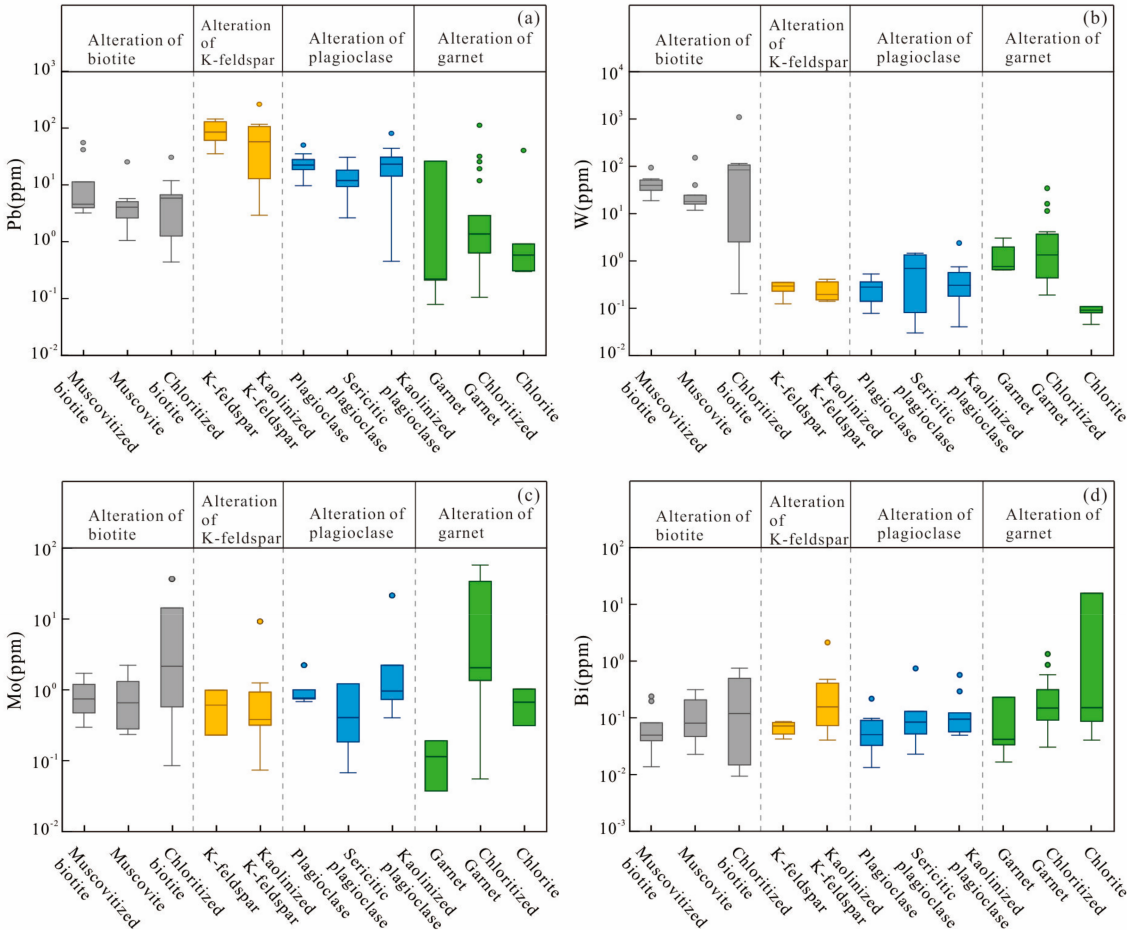

Figure 7. Box plots of (**a**) Pb, (**b**) W, (**c**) Mo and (**d**) Bi concentrations of the main silicate minerals and alteration minerals in granites and skarns.

6.2.3. Alteration of Biotite

Granite-hosted biotite is generally altered to muscovite and chlorite to varying degrees (Figure 4a,b).

The W contents decrease and the Pb, Mo and Bi contents are almost unchanged during the alteration of biotite to muscovite (Figure 7). Muscovite is a TOT-type phyllosilicate with the general formula $KAl_2[AlSi_3O_{10}][OH]_2$. Ti is a common trace element in both biotite and muscovite [48]. In this study, muscovitized biotite and muscovite contained TiO_2 ranging from 0.084–1.16 wt % and 0.017–9.11 wt %, respectively. Furthermore, W was speculated to reside in the lattice as an isomorphous substitution of Ti^{4+} at the octahedral site, based on their similar time-resolved LA-ICP-MS spectra (Figure 6j,k) and similar crystal chemical properties, with the substitution equation $Fe^{2+} + W^{6+} \rightarrow 2Ti^{4+}$ [50,66]. During the alteration process of biotite to muscovite, Al_2O_3 content remarkably increases, while FeO, MnO, CaO, MgO, TiO_2 and W contents decrease (Table S3, Figure 7b). As a result of this alteration, Al^{3+} likely enters octahedral-coordinate positions to replace Fe, Mg and Ti in muscovite. As a result of the isomorphous substitution of W and Ti, W may also be replaced by Al and thus may be leached by magmatic-hydrothermal fluids as supported by the lower W contents of hydrothermal muscovite. Moreover, Pb has no obvious correlations with other elements in muscovite

and muscovite-altered biotite. The time-resolved LA-ICP-MS spectra of Pb for muscovitized biotite and muscovite suggest that Pb occurs as an isomorphous substitution of K in the mineral lattice (Figure 6j,k).

Compared with muscovitized biotite, chloritized biotite has variable contents of TiO_2, Pb, W, Mo and Bi (Figure 7). As mentioned above, chlorite is a TOT-type phyllosilicate mineral. In this case, W was also speculated to reside in the lattice as an isomorphous substitution of Ti^{4+} at the octahedral site (Figure 6l). The spectra of Pb in chloritized biotite are covariant with K, which indicates that Pb occurs as an isomorphous substitution of K, with Pb content being rather low due to low K concentration. Chloritized biotite contains relatively low Bi contents as Bi^{3+} isomorphously substitutes Pb^{2+}. Finally, Mo occurs as Mo-bearing submicroscopic inclusions residing in the muscovite, muscovitized biotite and chloritized biotite (Figures 6j–l and 7d).

6.2.4. Alteration of Garnet

Garnet is partially altered to chlorite in skarns (Figure 4e). When garnet is altered to chlorite, Al, Fe, Mn and Mg contents markedly increase, while the Ca and Ti contents decrease (Table S3). In addition, Pb, W, Mo and Bi have no obvious correlations with other elements in chloritized garnet and vary widely, not obviously changing during the alteration (Figure 7).

6.3. Mineralization of Pb, W, Mo and Bi

The migration and mineralization of W are closely related to reducing F-rich environments [22,67]. In addition, Sn, Bi and Mo are the most common and important accessory elements in W-polymetallic deposits [68]. Enrichments of F and Cl in granitic magmas could decline the solidus line and decrease viscosity and density of magma to prolong its fractional crystallization and will highly activate massive incompatible elements (e.g., REE and Pb) and concentrate ore-forming elements (W, Mo and Bi) [22,69,70]. As a consequence, F^- and Cl^- bearing magmatic-hydrothermal fluids are significantly important in transporting ore-forming elements from granitic magmas during the final stages of crystallization [22,71,72].

The metallogenesis of the Shizhuyuan W-polymetallic deposit is considered to be driven directly by the intrusion of the Qianlishan granitic complex [8,16,19]. Previous studies characterized the Qianlishan granitic complex as being comprised of highly fractionated A-type granite and crystallized from highly reduced magma (source magma), which contains considerable highly volatile components including H_2O, F, B and Cl contents [16,22,71]. Previous studies indicated that there was a strong F complexation during the magmatic-hydrothermal evolution in the Shizhuyuan deposit [8,22]. Chen et al. [16] reported high F contents (up to 8690 ppm) in Qianlishan granites. Hydrothermal zircons from Qianlishan granites also implied that F-rich magmatic-hydrothermal fluid derived from granites played an important role in W-Sn mineralization of the Shizhuyuan deposit [19,22]. Exsolution of the magmatic-hydrothermal fluid from the source magma and the associated mineralization may be summarized as follows. At the beginning, the source magma ascended below the Shizhuyuan area due to the regional tectonic-magmatic process in the SCB, which was highly rich in F, B and Cl and accumulated W together with other ore-forming elements (e.g., Mo, Bi) [19,32]. The abundances of ore-forming elements may have been further enhanced by fractional crystallization (forming the Qianlishan granites) in reduced systems and thus formed the highly evolved late residual magmatic-hydrothermal fluids [16,19,73]. During the fractional crystallization, parts of Pb and W entered the lattice of feldspar and biotite as isomorphisms, respectively. When biotite and feldspar altered in the later magmatic-hydrothermal process, W enriched in biotite and Pb enriched in feldspar were excluded from the mineral lattice and did not enter the alteration products (e.g., muscovite and kaolinite, Figure 8). Thus, Pb and W were released into the magmatic-hydrothermal fluids. As the W-, Pb-, Mo- and Bi-bearing submicroscopic inclusions residing in the minerals were very tiny, they could easily enter the fluids during the alterations as well. In addition, W and F formed W-F complexes, such as WF_6 and decomposed to H_2WO_4 according to the reaction $WF_6 + 4H_2O \rightarrow H_2WO_4 + 6HF$,

which could react with Ca^{2+} to form scheelite [50]. Moreover, Mo readily formed strong, complexing anions, which were transported in the fluids in the form of oxyacid or oxysalt (such as $MoO_3 \cdot nH_2O$ and MoO_2Cl_2) due to the high electrovalence and small ionic radius [74]. In contrast, Pb mainly occurred in the fluids in the form of volatile chemical compounds (such as $PbCl_2$) [70]. In this case, large amounts of W were precipitated in scheelite when fluids came in contact with carbonate rocks to form skarn, while a few contents of Pb, Mo and Bi were distributed in the skarn minerals at the same stage. Thus, large amounts of Pb, Mo, Bi and residual W remained in the ore-forming fluids, resulting in the formation of a W-Sn-Mo-Bi massive skarn ore at a later stage [8,14].

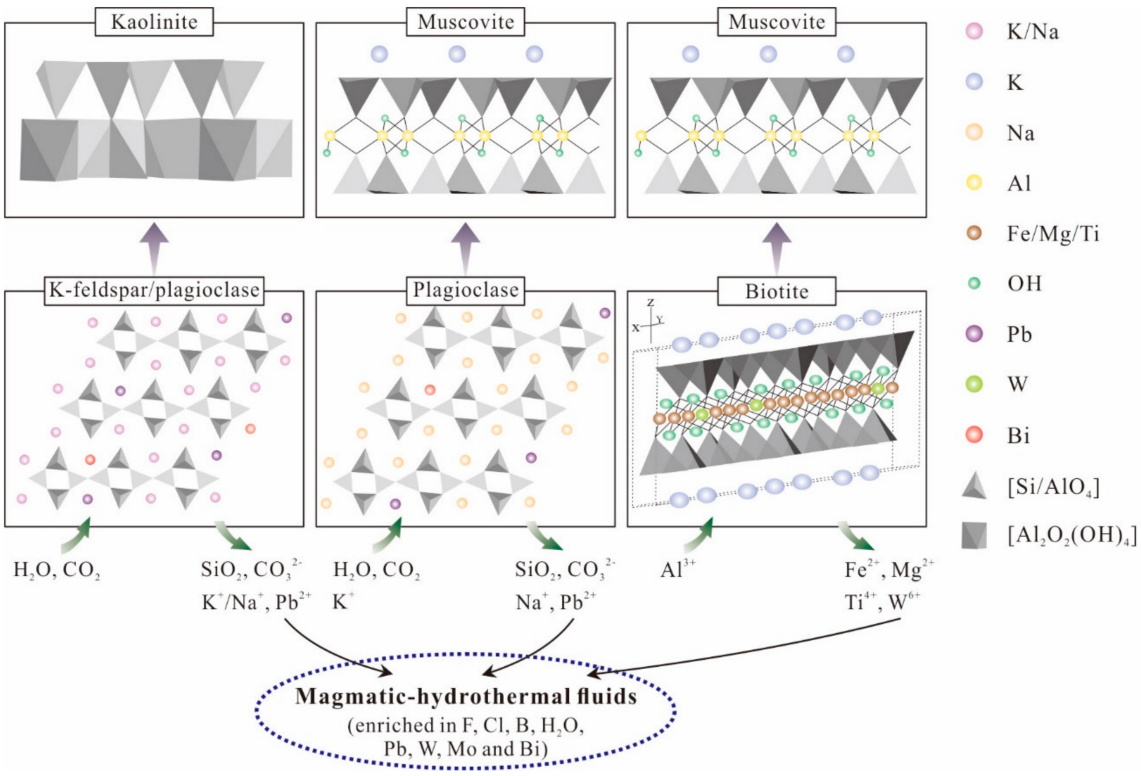

Figure 8. Alteration models for K-feldspar, plagioclase and biotite contributed to Pb, W, Mo and Bi mineralization of the Shizhuyuan W-polymetallic deposit.

7. Conclusions

W is mainly distributed in biotite and muscovitized biotite in the granite complex and scheelite in skarns. Pb is mainly distributed in feldspar in granites and epidote in skarns. Scheelite contains considerable amounts of W, Pb, Mo and Bi. Pb mainly occurs as an isomorphous substitution and is associated with K (i.e., in feldspar, micas and chlorite) or Ca (i.e., in scheelite and epidote) in minerals. W occurs as an isomorphous substitution and mainly correlates with Ti in biotite. Mo isomorphously substitutes W in scheelite with high content, while it may occur as Mo-bearing submicroscopic inclusions in silicate minerals with relatively low content. Bi mainly occurs as an isomorphous substitution of Pb when the Pb content is relatively high (such as in K-feldspar). When the Pb content is relatively low, Bi can occur as Bi-bearing micro or submicroscopic inclusions in minerals (such as in garnet).

During the later hydrothermal alteration (e.g., the alterations of biotite and feldspar), large amounts of W enriched in biotite and Pb enriched in feldspar were excluded from the mineral lattice and entered the magmatic-hydrothermal fluids. During the formation of the skarn deposits, a significant amount of W entered scheelite and few contents of Pb, Mo and Bi were precipitated in skarn minerals at the same stage. Thus, large amounts of Pb, Mo, Bi and residual W remained in the ore-forming fluids, resulting in the formation of W-Sn-Mo-Bi massive skarn ore at a later stage.

Supplementary Materials: The following are available online at http://www.mdpi.com/2075-163X/10/9/748/s1, Table S1: LA-ICP-MS analytical results for silicate minerals and scheelite from the Shizhuyuan W-polymetallic deposit (data of major elements for muscovitized biotite, chloritized biotite, muscovite, K-feldspar, kaolinized K-feldspar, plagioclase, sericitic plagioclase, kaolinized plagioclase, garnet, chloritized garnet, chlorite and epidote are cited from electronic Appendix C in Yuan et al. [13]), Table S2: LA-ICP-MS analytical results for international reference materials (data of major elements are cited from electronic Appendix B in Yuan et al. [13]), Table S3: Summary statistics of major elements, Pb, W, Mo and Bi concentrations for major silicate minerals as well as scheelite and alteration minerals (major elements for silicate minerals are cited from Yuan et al. [13]).

Author Contributions: Conceptualization, Q.H.; writing—original draft preparation, J.Y.; writing—review and editing, Q.H.; supervision and validation, Z.Y.; resources, Z.H.; formal analysis, T.Y. All authors have read and agreed to the published version of the manuscript.

Funding: This research was funded by the National Key R&D Program of China (2016YFC0600604 and 2017YFD0800304) and the China Geological Survey Project (12120113002300, DD20160323).

Acknowledgments: We gratefully acknowledge Zhimin Tang, Hua Jiang and Changyu Wang for sample collection and fieldwork. We also wish to thank Longxue Li, Lanchu Tao, Tao Luo, Wenning Lu and Qingshang Shi for their analytical assistance.

Conflicts of Interest: The authors declare no conflict of interest.

References

1. Zhao, P.; Zhao, H.; Yuan, S.; Mao, J. The Early Jurassic Fe–Sn metallogenic event and its geodynamic setting in South China: Evidence from Re–Os, U–Pb geochronology and geochemistry of the Dading magnesian skarn Fe–Sn deposit. *Ore Geol. Rev.* **2019**, *111*, 1–13. [CrossRef]
2. Sun, H.; Zhao, Z.; Yan, G.; Lü, Z.; Huang, Z.; Yu, X. Geological and geochronological constraints on the formation of the Jurassic Maozaishan Sn deposit, Dayishan orefield, South China. *Ore Geol. Rev.* **2018**, *94*, 212–224. [CrossRef]
3. Zhao, W.W.; Zhou, M.; Li, Y.; Zhao, Z.; Gao, J. Genetic types, mineralization styles, and geodynamic settings of Mesozoic tungsten deposits in South China. *J. Asian Earth Sci.* **2017**, *137*, 109–140. [CrossRef]
4. Zhou, M.; Gao, J.; Zhao, Z.; Zhao, W. Introduction to the special issue of Mesozoic W-Sn deposits in South China. *Ore Geol. Rev.* **2018**, *101*, 432–436. [CrossRef]
5. Cao, J.; Wu, Q.; Yang, X.; Kong, H.; Li, H.; Xi, X.; Huang, Q.; Liu, B. Geochronology and genesis of the Xitian W-Sn Polymetallic Deposit in eastern Hunan Province, South China: Evidence from zircon U-Pb and muscovite Ar-Ar dating, petrochemistry, and wolframite Sr-Nd-Pb isotopes. *Minerals* **2018**, *8*, 111. [CrossRef]
6. Mao, J.; Xie, G.; Guo, C.; Chen, Y. Large-scale tungsten-tin mineralization in the Nanling region, South China: Metallogenic ages and corresponding geodynamic processes. *Acta Petrol. Sin.* **2007**, *23*, 2329–2338.
7. Zhao, P.; Yuan, S.; Mao, J.; Yuan, Y.; Zhao, H.; Zhang, D.; Shuang, Y. Constraints on the timing and genetic link of the large-scale accumulation of proximal W–Sn–Mo–Bi and distal Pb–Zn–Ag mineralization of the world-class Dongpo orefield, Nanling Range, South China. *Ore Geol. Rev.* **2018**, *95*, 1140–1160. [CrossRef]
8. Lu, H.; Liu, Y.; Wang, C.; Xu, Y.; Li, H. Mineralization and fluid inclusion study of the Shizhuyuan W-Sn-Bi-Mo-F skarn deposit, Hunan province, Cehina. *Econ. Geol.* **2003**, *98*, 955–974. [CrossRef]
9. Mao, J.; Cheng, Y.; Chen, M.; Pirajno, F. Major types and time-space distribution of Mesozoic ore deposits in South China and their geodynamic settings. *Miner. Depos.* **2013**, *48*, 267–294. [CrossRef]
10. Yuan, S.; Peng, J.; Hu, R.; Li, H.; Shen, N.; Zhang, D. A precise U-Pb age on cassiterite from the Xianghualing tin-polymetallic deposit (Hunan, South China). *Miner. Depos.* **2008**, *43*, 375–382. [CrossRef]
11. Yuan, S.; Liu, X.; Wang, X.; Wu, S.; Yuan, Y.; Li, X.; Wang, T. Geological characteristics and ^{40}Ar-^{39}Ar geochronology of the Hongqiling tin deposit in southern Hunan Province. *Acta Petrol. Sin.* **2012**, *28*, 3787–3797, (In Chinese with English Abstract).
12. Yuan, S.; Zhang, D.; Shuang, Y.; Du, A.; Qu, W. Re-Os dating of molybdenite from the Xintianling giant tungsten-molybdenum deposit in southern Hunan Province, China and its geological implications. *Acta Petrol. Sin.* **2012**, *28*, 27–38, (In Chinese with English Abstract).
13. Yuan, J.; Hou, Q.; Yang, Z.; Jiang, H.; Hu, Z.; Yu, T. Distribution and mobilization of Sn in silicate minerals from the Mesozoic Shizhuyuan W-dominated polymetallic deposit, South China. *Ore Geol. Rev.* **2018**, *101*, 595–608. [CrossRef]
14. Mao, J.; Li, H.; Hidehiko, S.; Louis, R.; Bernard, G. Geology and metallogeny of the Shizhuyuan Skarn-Greisen Deposit, Hunan Province, China. *Int. Geol. Rev.* **1996**, *38*, 1020–1039.

15. Wu, L.; Hu, R.; Peng, J.; Bi, X.; Jiang, G.; Chen, H.; Wang, Q.; Liu, Y. He and Ar isotopic compositions and genetic implications for the giant Shizhuyuan W-Sn-Bi-Mo deposit, Hunan Province, South China. *Int. Geol. Rev.* **2011**, *53*, 677–690. [CrossRef]
16. Chen, Y.; Li, H.; Sun, W.; Ireland, T.; Tian, X.; Hu, Y.; Yang, W.; Chen, C.; Xu, D. Generation of Late Mesozoic Qianlishan A_2-type granite in Nanling Range, South China: Implications for Shizhuyuan W-Sn mineralization and tectonic evolution. *Lithos* **2016**, *266–267*, 435–452. [CrossRef]
17. Cheng, Y. Petrogenesis of skarn in Shizhuyuan W-polymetallic deposit, southern Hunan, China: Constraints from petrology, mineralogy and geochemistry. *Trans. Nonferrous Met. Soc. China* **2016**, *26*, 1676–1687. [CrossRef]
18. Huang, F.; Wang, R.; Xie, L.; Zhu, J.; Erdmann, S.; Che, X.; Zhang, R. Differentiated rare-element mineralization in an ongonite–topazite composite dike at the Xianghualing tin district, Southern China: An electron-microprobe study on the evolution from niobium–tantalum-oxides to cassiterite. *Ore Geol. Rev.* **2015**, *65*, 761–778. [CrossRef]
19. Jiang, W.; Li, H.; Mathur, R.; Wu, J. Genesis of the giant Shizhuyuan W-Sn-Mo-Bi-Pb-Zn polymetallic deposit, South China: Constraints from zircon geochronology and geochemistry in skarns. *Ore Geol. Rev.* **2019**, *111*, 1–22. [CrossRef]
20. Xie, L.; Wang, R.; Chen, J.; Zhu, J. Mineralogical evidence for magmatic and hydrothermal processes in the Qitianling oxidized tin-bearing granite (Hunan, South China): EMP and (MC)-LA-ICPMS investigations of three types of titanite. *Chem. Geol.* **2010**, *276*, 53–68. [CrossRef]
21. Yuan, S.; Peng, J.; Hao, S.; Li, H.; Geng, J.; Zhang, D. In situ LA-MC-ICP-MS and ID-TIMS U–Pb geochronology of cassiterite in the giant Furong tin deposit, Hunan Province, South China: New constraints on the timing of tin–polymetallic mineralization. *Ore Geol. Rev.* **2011**, *43*, 235–242. [CrossRef]
22. Jiang, W.; Li, H.; Evans, N.J.; Wu, J. Zircon records multiple magmatic-hydrothermal processes at the giant Shizhuyuan W–Sn–Mo–Bi polymetallic deposit, South China. *Ore Geol. Rev.* **2019**, *115*, 1–24. [CrossRef]
23. Liu, Y.; Hu, Z.; Gao, S.; Günther, D.; Xu, J.; Gao, C.; Chen, H. In situ analysis of major and trace elements of anhydrous minerals by LA-ICP-MS without applying an internal standard. *Chem. Geol.* **2008**, *257*, 34–43. [CrossRef]
24. Nadoll, P.; Koenig, A.E. LA-ICP-MS of magnetite: Methods and reference materials. *J. Anal. At. Spectrom.* **2011**, *26*, 1872–1877. [CrossRef]
25. Zhang, Z.; Xie, G.; Mao, J.; Liu, W.; Olin, P.; Li, W. Sm-Nd dating and in-situ LA-ICP-MS trace element analyses of scheelite from the Longshan Sb-Au Deposit, Xiangzhong Metallogenic Province, South China. *Minerals* **2019**, *9*, 87. [CrossRef]
26. Sun, X.; Ni, P.; Yang, Y.; Qin, H.; Chen, H.; Gui, C.; Jing, S. Formation of the Qixiashan Pb–Zn deposit in Middle-Lower Yangtze River Valley, eastern China: Insights from fluid inclusions and in situ LA-ICP-MS sulfur isotope data. *J. Geochem. Explor.* **2018**, *192*, 45–59. [CrossRef]
27. Yu, F.; Shu, Q.; Niu, X.; Xing, K.; Li, L.; Lentz, D.R.; Zeng, Q.; Yang, W. Composition of garnet from the Xianghualing Skarn Sn Deposit, South China: Its petrogenetic significance and exploration potential. *Minerals* **2020**, *10*, 456. [CrossRef]
28. Song, G.; Cook, N.J.; Li, G.; Qin, K.; Ciobanu, C.L.; Yang, Y.; Xu, Y. Scheelite geochemistry in porphyry-skarn W-Mo systems: A case study from the Gaojiabang Deposit, East China. *Ore Geol. Rev.* **2019**, *113*, 1–17. [CrossRef]
29. Choi, W.; Park, C.; Song, Y. Multistage W-mineralization and magmatic-hydrothermal fluid evolution: Microtextural and geochemical footprints in scheelite from the Weondong W-skarn deposit, South Korea. *Ore Geol. Rev.* **2020**, *116*, 1–24. [CrossRef]
30. Chen, F.; Deng, J.; Wang, Q.; Huizenga, J.M.; Li, G.; Gu, Y. LA-ICP-MS trace element analysis of magnetite and pyrite from the Hetaoping Fe-Zn-Pb skarn deposit in Baoshan block, SW China: Implications for ore-forming processes. *Ore Geol. Rev.* **2020**, *117*, 1–17. [CrossRef]
31. Yuan, S.; Mao, J.; Cook, N.J.; Wang, X.; Liu, X.; Yuan, Y. A Late Cretaceous tin metallogenic event in Nanling W-Sn metallogenic province: Constraints from U-Pb, Ar-Ar geochronology at the Jiepailing Sn-Be-F deposit, Hunan, China. *Ore Geol. Rev.* **2015**, *65*, 283–293. [CrossRef]

32. Zhang, R.; Lu, J.; Wang, R.; Yang, P.; Zhu, J.; Yao, Y.; Gao, J.; Li, C.; Lei, Z.; Zhang, W.; et al. Constraints of in situ zircon and cassiterite U–Pb, molybdenite Re–Os and muscovite ^{40}Ar–^{39}Ar ages on multiple generations of granitic magmatism and related W–Sn mineralization in the Wangxianling area, Nanling Range, South China. *Ore Geol. Rev.* **2015**, *65*, 1021–1042. [CrossRef]
33. Zaw, K.; Peters, S.G.; Cromie, P.; Burrett, C.; Hou, Z. Nature, diversity of deposit types and metallogenic relations of South China. *Ore Geol. Rev.* **2007**, *31*, 3–47. [CrossRef]
34. Jiang, Y.; Jiang, S.; Zhao, K.; Ling, H. Petrogenesis of Late Jurassic Qianlishan granites and mafic dykes, Southeast China: Implications for a back-arc extension setting. *Geol. Mag.* **2006**, *143*, 457–474. [CrossRef]
35. Yin, J.; Kim, S.; Lee, H.; Itay, T. K–Ar ages of plutonism and mineralization at the Shizhuyuan W–Sn–Bi–Mo deposit, Hunan Province, China. *J. Asian Earth Sci.* **2002**, *20*, 151–155. [CrossRef]
36. Zhao, Z.; Bao, Z.; Zhang, B.; Xiong, X. Crust-mantle interaction and its contribution to the Shizhuyuan superlarge tungsten polymetallic mineralization. *Sci. China. Ser. D* **2001**, *44*, 266–276. [CrossRef]
37. Guo, C.; Wang, R.; Yuan, S.; Wu, S.; Yin, B. Geochronological and geochemical constraints on the petrogenesis and geodynamic setting of the Qianlishan granitic pluton, Southeast China. *Miner. Petrol.* **2015**, *109*, 253–282. [CrossRef]
38. Liu, Y.; Hu, Z.; Zong, K.; Gao, C.; Gao, S.; Xu, J.; Chen, H. Reappraisement and refinement of zircon U-Pb isotope and trace element analyses by LA-ICP-MS. *Chin. Sci. Bull.* **2010**, *55*, 1535–1546. [CrossRef]
39. Lee, M.; Shin, D.; Yoo, B.; Im, H.; Pak, S.; Choi, S. LA-ICP-MS trace element analysis of arsenopyrite from the Samgwang gold deposit, South Korea, and its genetic implications. *Ore Geol. Rev.* **2019**, *114*, 1–16. [CrossRef]
40. Zhao, X.; Zhong, H.; Mao, W.; Bai, Z.; Xue, K. Molybdenite Re-Os dating and LA-ICP-MS trace element study of sulfide minerals from the Zijinshan high-sulfidation epithermal Cu-Au deposit, Fujian Province, China. *Ore Geol. Rev.* **2020**, *118*, 1–17. [CrossRef]
41. Radosavljevic-Mihajlovic, A.S.; Kremenovic, A.S.; Dosen, A.M.; Andrejic, J.Z.; Dondur, V.T. Thermally induced phase transformation of Pb-exchanged LTA and FAU-framework zeolite to feldspar phases. *Microporous Mesoporous Mater.* **2015**, *201*, 210–218. [CrossRef]
42. Railsback, L.B. An earth scientist's periodic table of the elements and their ions. *Geology* **2003**, *31*, 737–740. [CrossRef]
43. Chen, J.; Ke, B.; Lan, L.; Li, Y. Influence of Ag, Sb, Bi and Zn impurities on electrochemical and flotation behaviour of galena. *Miner. Eng.* **2015**, *72*, 10–16. [CrossRef]
44. George, L.; Cook, N.J.; Ciobanu, C.L.; Wade, B.P. Trace and minor elements in galena: A reconnaissance LA-ICP-MS study. *Am. Mineral.* **2015**, *100*, 548–569. [CrossRef]
45. Zhou, H.; Sun, X.; Fu, Y.; Lin, H.; Jiang, L. Mineralogy and mineral chemistry of Bi-minerals: Constraints on ore genesis of the Beiya giant porphyry-skarn gold deposit, southwestern China. *Ore Geol. Rev.* **2016**, *79*, 408–424. [CrossRef]
46. Zhang, J.; Deng, J.; Chen, H.; Yang, L.; Cooke, D.; Danyushevsky, L.; Gong, Q. LA-ICP-MS trace element analysis of pyrite from the Chang'an gold deposit, Sanjiang region, China: Implication for ore-forming process. *Gondwana Res.* **2014**, *26*, 557–575. [CrossRef]
47. Monier, G.; Robert, J.L. Evolution of the miscibility gap between muscovite and biotite solid solutions with increasing lithium content: An experimental study in the system K_2O-Li_2O-MgO-FeO-Al_2O_3-SiO_2-H_2O-HF at 600 °C, 2 kbar P_{H2O}: Comparison with natural lithium micas. *Mineral. Mag.* **1986**, *50*, 641–651. [CrossRef]
48. Wang, R.; Zhu, J.; Zhang, W.; Xie, L.; Yu, A.; Che, X. Ore-forming mineralogy of W-Sn granites in the Nanling Range: Concept and case study. *Geol. J. Chin. Univ.* **2008**, *14*, 485–495, (In Chinese with English Abstract).
49. Johan, Z.; Johan, V. Micas of the Cinovec (Zinnwald) granite cupola, Czech Republic: A new insight into Sn and W metallogenesis. *CR Acad. Sci. Paris* **2001**, *332*, 307–313.
50. Johan, Z.; Strnad, L.; Johan, V. Evolution of the Cinovec (Zinnwald) granite gupola, Czech Republic: Composition of feldspars and micas, a clue to the origin of W, Sn mineralization. *Can. Mineral.* **2012**, *50*, 1131–1148. [CrossRef]
51. Gaspar, M.; Knaack, C.; Meinert, L.D.; Moretti, R. REE in skarn systems: A LA-ICP-MS study of garnets from the Crown Jewel gold deposit. *Geochim. Cosmochim. Acta* **2008**, *72*, 185–205. [CrossRef]
52. Ganzhorn, A.C.; Pilorgé, H.; le Floch, S.; Montagnac, G.; Cardon, H.; Reynard, B. Deuterium-hydrogen inter-diffusion in chlorite. *Chem. Geol.* **2018**, *493*, 518–524. [CrossRef]

53. De Caritat, P.; Hutcheon, I.; Walshe, J.L. Chlorite geothermometry: A review. *Clays Clay Miner.* **1993**, *41*, 219–239. [CrossRef]
54. Yang, C.; Tang, J.; Song, J.; Zhang, Z.; Li, Y.; Sun, X.; Wang, Q.; Ding, S.; Fang, X.; Li, Y.; et al. Chlorite characteristic of the Naruo Porphyry Cu (Au) Deposit in Tibet and its geological significance. *Acta Geol. Sin.* **2015**, *89*, 856–872, (In Chinese with English Abstract).
55. Li, J.; Li, X.; Xiao, R. Multiple-stage tungsten mineralization in the Silurian Jiepai W skarn deposit, South China: Insights from cathodoluminescence images, trace elements, and fluid inclusions of scheelite. *J. Asian Earth Sci.* **2019**, *181*, 1–22. [CrossRef]
56. Hua, R.; Zhang, W.; Li, G.; Hu, D.; Wang, X. A preliminary study on the features and geologic implication of the accompanying metals in tungsten deposits in the Nanling Region. *Geol. J. Chin. Univ.* **2008**, *14*, 527–538, (In Chinese with English Abstract). [CrossRef]
57. Liu, J.; Li, W.; Zhu, X.; Zhou, J.; Yu, H. Ore genesis of the Late Cretaceous Larong porphyry W-Mo deposit, eastern Tibet: Evidence from in-situ trace elemental and S-Pb isotopic compositions. *J. Asian Earth Sci.* **2020**, *190*, 1–16. [CrossRef]
58. Su, S.; Qin, K.; Li, G.; Olin, P.; Thompson, J. Cathodoluminescence and trace elements of scheelite: Constraints on ore-forming processes of the Dabaoshan porphyry Mo-W deposit, South China. *Ore Geol. Rev.* **2019**, *115*, 1–18. [CrossRef]
59. Zhou, D.; Pang, L.; Wang, D.; Guo, H.; Yang, F.; Qi, Z.; Li, C.; Jin, B.; Reaney, I.M. Crystal structure, impedance and broadband dielectric spectra of ordered scheelite-structured $Bi(Sc_{1/3}Mo_{2/3})O_4$ ceramic. *J. Eur. Ceram. Soc.* **2018**, *38*, 1556–1561. [CrossRef]
60. Yuan, J.; Yang, J.; Ma, H.; Su, S.; Chang, Q.; Komarneni, S. Hydrothermal synthesis of nano-kaolinite from K-feldspar. *Ceram. Int.* **2018**, *44*, 15611–15617. [CrossRef]
61. Zhang, S.; Zhang, H. A discussion on the dynamic process of kaolinization of feldspar. *Acta Mineral. Sin.* **1992**, *12*, 373–379, (In Chinese with English Abstract).
62. Cora, I.; Dódony, I.; Pekker, P. Electron crystallographic study of a kaolinite single crystal. *Appl. Clay Sci.* **2014**, *90*, 6–10. [CrossRef]
63. Yuan, G.; Cao, Y.; Schulz, H.M.; Hao, F.; Gluyas, J.; Liu, K.; Yang, T.; Wang, Y.; Xi, K.; Li, F. A review of feldspar alteration and its geological significance in sedimentary basins: From shallow aquifers to deep hydrocarbon reservoirs. *Earth-Sci. Rev.* **2019**, *191*, 114–140. [CrossRef]
64. Li, S.; Xu, H.; Shen, J.; Li, G. *Crystallography and Mineralogy*; Geological Publishing House: Beijing, China, 2008; pp. 240–254. (In Chinese)
65. Huang, S.; Huang, K.; Feng, W.; Tong, H.; Liu, L.; Zhang, X. Mass exchanges among feldspar, kaolinite and illite and their influences on secondary porosity formation in clastic diagenesis—A case study on the Upper Paleozoic, Ordos Basin and Xujiahe Formation, Western Sichuan Depression. *Geochimica* **2009**, *38*, 498–506, (In Chinese with English Abstract).
66. Ye, L.; Bao, T.; Liu, Y.; He, F.; Wang, X.; Zhang, Q.; Wang, D.; Lan, J. The trace and rare earth elements in scheelites and their implication for the mineralization in Dulong Sn-Zn polymetal ore deposit, Yunnan Province. *J. Nanjing Univ. (Nat. Sci.)* **2018**, *54*, 245–258, (In Chinese with English Abstract). [CrossRef]
67. Wang, H.; Feng, C.; Li, D.; Xiang, X.; Zhou, J. Sources of granitoids and ore-forming materials of Dahutang tungsten deposit in northern Jiangxi Province: Constraints from mineralogy and isotopic tracing. *Acta Petrol. Sin.* **2015**, *31*, 725–739, (In Chinese with English Abstract).
68. Liu, Y.; Cheng, Q.; Xia, Q.; Wang, X. Mineral potential mapping for tungsten polymetallie deposits in the Nanling Metallogenic Belt, South China. *J. Earth Sci.* **2014**, *25*, 689–700. [CrossRef]
69. Park, C.; Song, Y.; Chung, D.; Kang, I.M.; Khulganakhuu, C.; Yi, K. Recrystallization and hydrothermal growth of high U-Th zircon in the Weondong deposit, Korea: Record of post-magmatic alteration. *Lithos* **2016**, *260*, 268–285. [CrossRef]
70. Webster, J.D.; Holloway, J.R. Partitioning of F and Cl between magmatic hydrothermal fluids and highly evolved granitic magmas. *Geo. Soc. Am. Spec. Pap.* **1990**, *246*, 20–34. [CrossRef]
71. Chen, B.; Ma, X.; Wang, Z. Origin of the fluorine-rich highly differentiated granites from the Qianlishan composite plutons (South China) and implications for polymetallic mineralization. *J. Asian Earth Sci.* **2014**, *93*, 301–314. [CrossRef]
72. Zhao, B.; Zhang, D.; Zhang, R.; Shi, C. The progress of geochemical properties and metallogenic effect of F-rich silicate melt-solution fluid system. *Chin. J. Geol.* **2015**, *50*, 222–240, (In Chinese with English Abstract).

73. Lehmann, B. *Metallogeny of Tin*; Springer: Berlin, Germany, 1990.
74. Rempel, K.U.; Williams-Jones, A.E.; Migdisov, A.A. The solubility of molybdenum dioxide and trioxide in HCl-bearing water vapour at 350 °C and pressures up to 160 bars. *Geochim. Cosmochim. Acta* **2008**, *72*, 3074–3083. [CrossRef]